Ru layers electrodeposited onto highly stable Ti_2AlC substrates as cathodes for hydrogen evolution in sulfuric acid solutions

B.M. Jović, V.D. Jović, U.Č. Lačnjevac, S.I. Stevanović, J. Kovač, M. Radovic, N.V. Krstajić

PII: S1572-6657(16)30039-X
DOI: doi: 10.1016/j.jelechem.2016.01.038
Reference: JEAC 2480

To appear in: *Journal of Electroanalytical Chemistry*

Received date: 25 November 2015
Revised date: 26 January 2016
Accepted date: 29 January 2016

Please cite this article as: B.M. Jović, V.D. Jović, U.Č. Lačnjevac, S.I. Stevanović, J. Kovač, M. Radovic, N.V. Krstajić, Ru layers electrodeposited onto highly stable Ti_2AlC substrates as cathodes for hydrogen evolution in sulfuric acid solutions, *Journal of Electroanalytical Chemistry* (2016), doi: 10.1016/j.jelechem.2016.01.038

Ru layers electrodeposited onto highly stable Ti_2AlC substrates as cathodes for hydrogen evolution in sulfuric acid solutions

B.M. Jović[a], V.D. Jović[a], U.Č. Lačnjevac[a,*], S.I. Stevanović[b], J. Kovač[c], M. Radović[d], N.V. Krstajić[e]

[a] *Institute for Multidisciplinary Research, University of Belgrade, Kneza Višeslava 1, 11030 Belgrade, Serbia*

[b] *Department of Electrochemistry, ICTM, University of Belgrade, Njegoševa 12, 11000 Belgrade, Serbia*

[c] *Department of Surface Engineering and Optoelectronics, Jožef Stefan Institute, Jamova 39, 1000 Ljubljana, Slovenia*

[d] *Department of Materials Science and Engineering, Texas A&M University, College Station, TX 77843, USA*

[e] *Faculty of Technology and Metallurgy, University of Belgrade, Karnegijeva 4, 11000 Belgrade, Serbia*

Abstract

In this work, the hydrogen evolution reaction (HER) was studied on Ru coated Ti_2AlC electrodes in 1.0 mol dm^{-3} H_2SO_4 at 25 °C. Ti_2AlC was found to be a highly stable substrate in sulfuric acid solutions due to the formation of a passivating oxide layer on the surface, which was confirmed by the X-ray photoelectron spectroscopy (XPS) analysis of as-prepared and anodically treated Ti_2AlC samples. Ru films were electrodeposited onto Ti_2AlC substrates by cycling the potential of Ti_2AlC in the solution containing 0.01 mol dm^{-3} $RuCl_3$ + 0.1 mol dm^{-3} H_2SO_4 between -0.5 V and 0.4 V vs. saturated calomel electrode (SCE) at the sweep rate of 20 mV s^{-1}. Four Ru/Ti_2AlC samples were prepared, obtained at 5, 10, 15 and 20 cycles of Ru electrodeposition. Characterization of samples was performed by scanning electron microscopy (SEM) and cyclic voltammetry (CV), while the thickness of the electrodeposited Ru layers was

* Corresponding author: Tel. +381-11-2085039; Fax. +381-11- 3055289

E-mail address: uros.lacnjevac@imsi.bg.ac.rs (U.Č. Lačnjevac)

determined by atomic force microscopy (AFM). It was found that the most compact sample with the thickness of about 0.42 μm was obtained after 5 cycles. Electrochemical impedance spectroscopy (EIS) and steady-state polarization measurements showed that all Ru/Ti_2AlC electrodes were exceptionally active for the HER. A Tafel slope of about -60 mV dec^{-1} was observed on all polarization curves in the range of high cathodic current densities. Based on the formal kinetics analysis, an appropriate mechanism for the HER on Ru/Ti_2AlC was suggested.

Key words: Ti_2AlC; electrodeposited Ru; H_2 evolution; acid solution; electrochemical impedance spectroscopy; cyclic voltammetry.

1. Introduction

Although the discovery of electrolytic water decomposition was first observed in acidic water [1], the electrode materials for water electrolysis were mainly developed for alkaline electrolytes, due to the fact that electrode materials for water electrolysis in acid electrolytes are mainly the noble metals, which are very expensive. Typical polymer electrolyte membrane water electrolyzers (PEMWEs) operating in acidic environments employ the Pt catalyst loaded on the carbon black support at the cathode side [2]. Besides Pt, one of the most investigated HER catalysts are the Ru based materials, namely Ru oxides, which display excellent activity for the HER both in alkaline [3-8] and acidic media [7,9-14]. However, widely used carbon supports, although possessing a high surface area and sufficient electronic conductivity, are prone to corrosion and degradation during the electrolysis, which has a detrimental effect on the performance of the Pt/C catalyst layer and increases the overall production costs. Consequently, further research effort regarding the development of more durable and efficient supporting materials for HER electrocatalysts in PEMWE conditions is required.

Promising substrate materials were found to be the MAX phases. The MAX phases, $M_{(n+1)}AX_n$ ternary carbides and nitrides (where M is an early transition metal, A is an A group element, X is C, N and *n*D1–3) belong to the family of more than 50 layered hexagonal (space

group P63/mmc) compounds [15,16]. It is fairly well established by now that these phases belong to a new class of solids with an unusual, and sometimes unique, set of properties [15,17-19]. Some of them, like Ti_2AlC, are exceptionally oxidation resistant and are candidate materials for high temperature structural industrial applications [20,21]. They are excellent electrical and thermal conductors. Unlike early transition metal binary carbides, they are all relatively soft (Vickers hardness ≈ 2 to 5 GPa), most readily machinable [22] and can be easily fabricated and machined in any desired shape [15,16].

Recently, corrosion behavior of the MAX phases has drawn attention of the research community because some of them form stable passive layers in different acidic and alkaline solutions with no applied current/potential [23,24], while some of them exfoliate forming 2D binary carbides (MXenes) [25,26]. Exfoliation was found to be typical for Ti_3AlC_2 after prolonged exposure to 10% HF solution. The first comprehensive study on corrosion response of one of the MAX phases, namely Ti_3SiC_2, in HCl and H_2SO_4 [27,28] showed that in both acids, under open circuit conditions as well as at high anodic potentials, Ti leaches out from the substrate, while Si oxidizes in situ to form a SiO_2-based oxide that passivates the surface. In the case of Ti_3GeC_2, the passive layer was found to be GeO_2 [29].

Corrosion behavior of Ti_2AlC, $(Ti,Nb)_2AlC$, V_2AlC, V_2GeC, Cr_2AlC, Ti_2AlN, Ti_4AlN_3, Ti_3SiC_2 and Ti_3GeC_2 in 1 mol dm^{-3} NaOH, 1 mol dm^{-3} HCl and 1 mol dm^{-3} H_2SO_4 solutions has also been investigated in the work by Jović et al. [30]. Polarization characteristics in 1 mol dm^{-3} NaOH reported in that study showed that V_2AlC, V_2GeC and Cr_2AlC underwent active dissolution at potentials more positive than the corrosion potential, while Ti_2AlC, $(Ti,Nb)_2AlC$, Ti_3SiC_2 and Ti_3GeC_2 passivated. On the other hand, in 1 mol dm^{-3} HCl solution, Ti_2AlC, V_2AlC and V_2GeC actively dissolved, while Ti_3SiC_2 and Ti_3GeC_2 passivated. Depending on potential, $(Ti,Nb)_2AlC$ and Cr_2AlC showed trans-passive behavior. In 1 mol dm^{-3} H_2SO_4 solution, Ti_2AlC, $(Ti,Nb)_2AlC$, Ti_3SiC_2 and Ti_3GeC_2 passivated, V_2AlC and V_2GeC showed active dissolution,

while Cr_2AlC exhibited trans-passive behavior. Ti_2AlN and Ti_4AlN_3 were found to be passive in all solutions except in 1 mol dm^{-3} HCl, where Ti_2AlN showed trans-passive behavior.

In this work an attempt was made to electrodeposit Ru layers onto Ti_2AlC substrates and investigate the HER on such coatings in 1.0 mol dm^{-3} H_2SO_4 solution. To the best of our knowledge, this is the first study to report the application of the Ti_2AlC MAX phase as a substrate material in the HER electrocatalysis.

2. Experimental

2.1. Preparation of dense Ti_2AlC

Spark Plasma Sintering (SPS25-10, Thermal Technology LLC, USA) was used to fabricate high density samples from MAXthal 211 commercial powder (Sandvik Heating Technology, Sweden). In short, the as-received powders were mounted in a graphite die and placed inside the SPS chamber. The sample was heated to 1300°C at 50°C min-1 for 15 minutes under an applied pressure of 100 MPa and cooled near to room temperature at a rate of 50 °C min^{-1}. The density of the sintered samples was >98% of theoretical, measured by the alcohol immersion method (200 proof ethanol) based on Archimedes' principle, using the procedure that is described in more detail elsewhere [31,32]. X-Ray diffraction (XRD) and scanning electron microscopy (SEM) results (not shown here) confirmed that samples contained around 7 vol% of impurities, mostly $TiAl_x$ and Al_2O_3, which were also present in as-received powders. The average grain length of 4.2 ± 2.5 µm and thickness of 2.1 ± 1 µm was measured from SEM images of the polished and etched samples.

2.2. Preparation of Ru layers on Ti_2AlC

Rectangular Ti_2AlC substrate samples with a thickness of 2 mm were connected to the Pt wire on the back side using silver paste and sealed in epoxy resin, so that only the front surface was exposed to the solution. Before Ru electrodeposition, the surface of Ti_2AlC substrates was

subsequently polished with emery papers 600, 1200, 2400 and 4000 and kept in an ultrasonic bath for 10 min to remove traces of polishing. Ru layers were electrodeposited by cycling the sealed Ti_2AlC substrate from -0.5 V to 0.4 V vs. SCE at the sweep rate of 20 mV s^{-1} in the solution containing 0.01 mol dm^{-3} $RuCl_3$ + 0.1 mol dm^{-3} H_2SO_4 [33]. Four samples, obtained at 5, 10, 15 and 20 cycles, were prepared and marked as Ru5, Ru10, Ru15 and Ru20 in the text, respectively.

2.3. Physicochemical characterization

The X-ray photoelectron spectroscopy (XPS) analysis of as-prepared and electrochemically oxidized Ti_2AlC samples was carried out on a PHI-TFA XPS spectrometer (Physical Electronics Inc.) in ultra-high vacuum. The analyzed area was approximately 0.4 mm in diameter and was about 3-5 nm deep. Sample surfaces were excited by X-ray radiation from a monochromatic Al source at photon energy of 1486.6 eV. Quantification of surface composition was performed from XPS peak intensities taking into account relative sensitivity factors provided by the instrument manufacturer [34]. In order to analyze in-depth distribution of elements in the sub-surface region extending up to 50 nm below the surface, the XPS depth profiling was performed in combination with ion sputtering. The Ar ions of energy 3 keV were used. The velocity of the ion sputtering was estimated to be 2.0 nm/min calibrated on the Ni/Cr multilayer structure of a known thickness.

The surfaces of the Ru5, Ru10, Ru15 and Ru20 samples were investigated by SEM (Tescan VEGA TS 5130MM), while the thickness of each Ru electrodeposit was determined by AFM, NanoScope 3D (Veeco, USA) microscope operated in contact mode under ambient conditions. Silicon nitride probes with the spring constant of 20-60 N/m were used in this analysis. The thicknesses of the coatings (d) were determined at four different positions and the average values are presented.

2.4. Electrochemical measurements and solutions

Electrochemical measurements were performed onto Ti_2AlC and Ru5, Ru10, Ru15 and Ru20 samples in a 1.0 mol dm^{-3} H_2SO_4 solution in extra pure UV water (Smart2PureUV, TKA) at 25 °C. A three-compartment cell was used. The working electrode was placed in a central compartment together with the Luggin capillary, while a Pt mesh counter electrode of a larger surface area was placed in a separate compartment (parallel to the working electrode), so that oxygen evolved at the counter electrode could not enter the working electrode compartment. The SCE was placed in a side compartment connected to the central one through a bridge and a Luggin capillary, and was kept at the room temperature. All values of potential in the text are given versus the SCE (E_{SCE} = +0.244 V vs. the standard hydrogen electrode (SHE) at 25 °C). Experiments were performed using the potentiostat Reference 600 and the software PHE 200 and DC 105 (Gamry Instruments). All samples were first submitted to the HER at a constant current density j = -0.3 A cm^{-2} for 800 s (step 1), followed by the HER at a constant potential for 60 s (step 2). The value of potential in step 2 was adjusted to produce a cathodic current density slightly higher than -0.3 A cm^{-2}. After such pre-electrolysis, polarization curves were recorded by sweeping the potential with 1 mV s^{-1} from the potential applied in step 2 to the value slightly more positive than the open circuit potential (OCP). Potential was automatically corrected for the *IR* drop using the current interrupt technique.

EIS measurements were conducted with the same potentiostat and EIS 300 software, applying the amplitude of 5 mV RMS in the frequency range from 10 kHz to 0.01 Hz with 20 points per decade. EIS spectra were recorded at five different potentials for each sample. The real (Z') and imaginary (Z'') components of electrochemical impedance spectra in the Nyquist plot were analyzed using the complex nonlinear least squares (CNLS) fitting program (EIS 300) to simulate the equivalent resistances and capacitances.

3. Results and Discussion

3.1. Characterization of Ti_2AlC substrates

Ti_2AlC substrates were tested in a 1.0 mol dm^{-3} H_2SO_4 solution by recording polarization curves in a wide range of potentials negative and positive of the OCP, i.e. from -1.00 V to 2.00 V. The typical polarization curve is shown in Fig. 1. As can be seen, the OCP was established at a potential of -0.25 V, almost equal to the equilibrium potential of the hydrogen reaction. However, it is obvious that Ti_2AlC exhibits poor HER activity in an acidic medium. The HER on Ti_2AlC was characterized by a Tafel slope of -120 mV dec^{-1}, reaching a current density of about -400 mA cm^{-2} at potentials as negative as -1.00 V. At the same time, Ti_2AlC was found to be very stable during the HER, since neither hydride formation nor surface destruction was observed after prolonged hydrogen evolution. For example, after 10 days of hydrogen evolution in 1.0 mol dm^{-3} H_2SO_4 at a current density of -300 mA cm^{-2}, no SEM (not shown here) visible changes were recorded on the surface of Ti_2AlC. At potentials more positive than the OCP, Ti_2AlC displayed typical passivation behavior up to the higher potential limit of 2.00 V [30], characterized by a passivation current density of about 100 µA cm^{-2} (Fig. 1). It appears that the thin oxide film formed at anodic potentials suppresses oxygen evolution, as well as the corrosion of Ti_2AlC electrodes in 1.0 mol dm^{-3} H_2SO_4 solution.

It has been documented that one of the main reasons for decreasing activity and stability of HER cathodes under long term operation in industrial chlor-alkali electrolysis systems is the occurrence of reversed polarity of the electrodes, which takes place during the replacement of old electrodes of the zero-gap electrolyzer cells with the new ones. When this procedure is applied to one set of the cells, anodes and cathodes of the rest of cells are short-circuited, causing a reverse current flow [35-37]. Under such conditions, high anodic potentials are established on nominal cathodes in the electrolyzer, which can damage the cathode materials and cause a loss in their activity for the HER. Similar behavior of HER cathodes might be expected during the electrode replacement procedure in PEMWE systems. In order to determine the composition of Ti_2AlC surface layers formed under reversed polarity conditions, XPS analysis was performed

on two Ti_2AlC samples: the as-prepared one and the Ti_2AlC sample subjected to a potential of 2.0 V in 1.0 mol dm^{-3} H_2SO_4 for 1 hour. Figure 2 shows XPS depth profiles (concentration of elements as a function of depth) of the surface region for the non-treated (a) and the anodically treated sample (b). The surface of both samples was covered by a 2 nm thick carbon-rich layer. However, the non-treated sample had a much higher concentration of C at the surface (71 at.%), which can be attributed to the existence of a contamination layer on this sample. The C concentration was comparatively lower at the anodically treated sample (40 at.%), most probably as a consequence of oxidative removal of carbon-based species from the sample surface. Beneath the carbon-rich layer an oxygen-containing layer was present with the maximum concentration of O at a depth of about 3 nm for both samples. In the anodically treated sample the maximum was higher (51 at.%) than in the as-prepared sample (46 at.%). At greater depths the level of the O concentration decreases for both samples, but the O content in the inner part of the anodically treated sample was markedly higher than that for the as-prepared sample. This confirms that the surface region of Ti_2AlC was oxidized during the anodic polarization treatment. Interestingly, the curves for the O concentration do not decrease to 0 at.% with increasing depth as one would expect for the inner part of the samples, especially for non-treated Ti_2AlC. The phenomenon of O incorporation in the Ti_2AlC has been theoretically predicted and calculated [38-40], as well as experimentally documented [41,42] in the literature. Hence, we cannot estimate the exact thickness of the oxide-containing layers from the XPS depth profiles, but only conclude that the oxide region on the anodically treated sample was thicker. As can be seen from Fig. 2, the concentration curves for Ti, Al and C follow expected behaviour inside the bulk of the samples. A slight discrepancy of the concentration curves from the stoichiometric ratio for Ti_2AlC may be an artefact of the XPS method (due to the presence of $TiAl_x$ and Al_2O_3 impurities), related to preferential sputtering of some elements from the surface during depth profiling and a modification of the analyzed composition.

Detailed analyses of the XPS spectra Ti 2p, Al 2p and C 1s, presented in Fig. 3, suggest that Ti atoms were oxidized in the surface region of both samples (Ti 2p peak at 458.6 eV), but beneath this layer the Ti atoms were bonded in carbide characterized by Ti 2p binding energy of 454.5 eV (Fig. 3a) [34,43]. The Al atoms on the surface of both samples were also mainly oxidized (Al 2p peak at 74.3 eV) (Fig. 3b). Unfortunately, the chemical sensitivity of the XPS method is not high enough to distinguish the binary compound Ti-Al-oxide from Ti-oxide/Al-oxide to determine more precisely the nature of the thin oxide layer. In addition, a small peak emerging at ~ 71.8 eV in the Al 2p spectra originates from the Al-carbide species from a deeper subsurface region [43]. The XPS carbon spectra C 1s from the surface of both samples (Fig. 3c) have the most intense peak at 284.8 eV related to the C-C/C-H bonds, but deeper than 2 nm all carbon atoms were bounded in carbides (C 1s peak at 281.5 eV) [43].

It can be concluded that the structure of Ti_2AlC is maintained under anodic polarization in sulphuric acid solutions, since active dissolution of Ti and Al is prevented by the formation of a thin, stable oxide layer at the surface. Such behavior indicates that Ti_2AlC could be a good substrate material for application in the HER electrocatalysis in H_2SO_4 solutions. Hence, Ti_2AlC was chosen as a substrate for electrodeposition of electrocatalytic Ru coatings.

3.2. Electrodeposition of Ru films

Following the procedure explained in Ref. [33] for electrodeposition of nanometric layers of Ru on glassy carbon substrates, four Ru/ Ti_2AlC samples, electrodeposited with 5, 10, 15 and 20 cycles at 20 mV s^{-1}, were prepared. In Fig. 4 are shown CVs corresponding to the preparation of samples with 5 (a) and 20 (b) Ru electrodeposition cycles (samples Ru5 and Ru20, respectively). Since the HER proceeds at potentials more negative than -0.3 V (equilibrium potential for the hydrogen reaction in 0.1 mol dm^{-3} H_2SO_4), the electrodeposition of Ru took place together with the HER. It can be seen that the maximum cathodic current density at the lower potential limit of -0.50 V and the voltammetric responses at potentials positive than -0.25

V (insets) increased with the number of performed cycles, indicating an increase in both the amount of electrodeposited Ru and its surface area.

3.3. Microstructure characterization of Ru/Ti_2AlC samples

The surface microstructure of samples Ru5, Ru10, Ru15 and Ru20 can be seen in SEM images shown in Fig. 5. All Ru/Ti_2AlC samples were characterized by the presence of uncovered Ti_2AlC substrate surfaces and/or holes in the Ru coating, as illustrated in Fig. 5a for sample Ru5. The holes presumably emerged at positions corresponding to entrapped hydrogen bubbles, but their appearance could also be related to the presence of impurities at the Ti_2AlC surface (Ti_2AlC purity was 93%) suppressing the Ru electrodeposition or causing poor adhesion of Ru deposits. The Ru deposit obtained for the lowest number of cycles was the most compact (Fig. 5b), but as the number of electrodeposition cycles increased, the cracks in the Ru coatings became more pronounced and larger parts of the Ru film peeled off from the Ti_2AlC substrate (Fig. 5c-h). This behavior is most probably the consequence of high residual stresses in the Ru coatings of higher thickness, promoted by intensive hydrogen evolution during the CV electrodeposition of Ru.

AFM analysis was employed in order to estimate the thickness of the Ru coatings. After detecting an uncovered Ti_2AlC substrate surface or a hole in the coating (see surface plots), section analysis was performed and the thickness of the Ru coating was measured. Two examples are shown in Fig. 6, for samples Ru5 (a-c) and Ru20 (d-f). The thickness of the coatings (d) was determined at four different positions and the average values (d_{av}) are presented in Table 1. As can be seen, the thickness of the Ru coatings increased with increasing the number of cycles for their electrodeposition, reaching almost 3 μm for Ru20. At hole-free surfaces of the coatings, the average height between the lowest and the highest point in the profile was about 60 nm for sample Ru5 and about 500 nm for sample Ru20, confirming that the roughness of Ru electrodeposit also increased with the number of cycles.

3.4. CV characterization of Ru/Ti_2AlC samples

Cyclic voltammetry characterization of the electrodeposited Ru film samples was performed in a 1.0 mol dm^{-3} H_2SO_4 solution at 25 °C by recording CVs at a sweep rate of 20 mV s^{-1} in the potential range from -0.25 to 0.40 V corresponding to the reversible Ru oxide formation [44]. The obtained CVs presented in Fig. 7a are very similar to those recorded on the bulk Ru electrodes in sulfuric acid solutions [44]. Well-defined peaks corresponding to underpotential hydrogen adsorption/desorption on/from metallic Ru [44] could be detected between -0.25 V and 0.0 V. It can be clearly seen that the peaks increased with the increasing number of electrodeposition cycles, indicating an increase of the electrochemically active surface area of electrodeposited Ru, as it was also suggested by the AFM analysis. After correction of measured voltammetric current densities for the roughness factor (r_f – see Section 3.5.), the CVs for different Ru/Ti_2AlC samples practically overlapped (Fig. 7b), confirming the dominant influence of surface roughness on the voltammetric responses.

3.5. EIS analysis of the HER

EIS measurements were performed on all four Ru/Ti_2AlC samples at five different potentials: -0.28, -0.30, -0.32, -0.33 and -0.34 V, covering a HER current density range from about -1 mA cm^{-2} to about -50 mA cm^{-2}. Figure 8 shows Nyquist plots recorded at potentials E = -0.28 V (a) and -0.34 V (b) for all samples, and Nyquist plots recorded on sample Ru15 at all five selected potentials (c). Experimental points are presented with symbols (squares, circles, triangles etc.), while theoretical curves obtained from the modeling are presented with lines. The Nyquist plots recorded at less negative potentials (-0.28 V in particular) possess two well-defined semicircles, while those recorded at more negative potentials are characterized by only one apparent arc or semicircle (except for Ru15), as illustrated in Fig. 8. The best fits for all samples at less negative potentials were obtained using the equivalent circuit presented in Fig. 9a, typical for the HER [45]. The HER kinetics-related part of this circuit consists of elements

$R_p \| CPE_p$ in series with R_{ct}, where the resistance R_p and the constant phase element CPE_p represent parameters associated with the relaxation of the adsorbed reaction intermediate upon potential perturbation [46], and R_{ct} is the charge transfer resistance. The remaining two elements in the circuit are the constant phase element CPE_{dl}, which usually replaces C_{dl} on solid electrodes, and the solution resistance R_s. The impedances of CPE_{dl} and CPE_p are given as:

$$Z_{CPE_{dl}} = \frac{1}{Y_{dl}(j\omega)^{\alpha_{dl}}}; Z_{CPE_p} = \frac{1}{Y_p(j\omega)^{\alpha_p}} \quad (1)$$

where Y_{dl} and Y_p are capacitance parameters (in Ω^{-1} cm^{-2} s^{α}), and α_{dl} and α_p are parameters associated with a constant phase angle $\varphi = -(90\alpha)°$, which may have a value between 0 and 1. This model predicts the occurrence of two semicircles: one at high frequencies originating from the elements $R_{ct} \| CPE_{dl}$, and the other at low frequencies corresponding to the elements $R_p \| CPE_p$ (Fig. 8a). At more negative potentials the contribution of parameters R_p and Y_p (CPE_p) to the total impedance response was negligible for most samples, so the model used for fitting was reduced to the simple Randles circuit presented in Fig. 9b. Only the impedance spectra of sample Ru15 displayed the characteristics of two time constants at all potentials (Fig. 8c) and were successfully fitted with the more complex equivalent circuit (Fig. 9a). Parameters obtained from the fitting procedure are presented in Table 2.

Values of C_{dl} were calculated using the equation [47]:

$$C_{dl} = \left[Y_{dl} \left(\frac{1}{R_s} + \frac{1}{R_{ct}} \right)^{(\alpha_{dl}-1)} \right]^{1/\alpha_{dl}} \quad (2)$$

The dependence of C_{dl} on potential for various Ru/Ti_2AlC samples is graphically presented in Fig. 10a. It can be observed that C_{dl} of all electrodes were constant in the investigated potential range, indicating an efficient detachment of evolved hydrogen bubbles from the Ru electrode surface. The obtained values for C_{dl} confirm that repetitive electrodeposition cycling produced Ru films with increasing surface roughness. In order to estimate the average roughness factor for the samples, calculated values of C_{dl} were divided by 20 μF cm^{-2} (the value of an

ideally flat electrode [48]) and corresponding results are given in Table 1 as r_f. It can be seen that the real surface area of the sample obtained after 20 cycles exhibited a four-fold increase compared with that of the sample obtained after 5 cycles.

The reciprocal value of the faradaic resistance, $1/R_F$ ($R_F = R_{ct} + R_p$), can be regarded as a direct measure of the electrode activity for the HER. Figure 10b shows the E vs. log R_F^{-1} dependences obtained for all samples from the EIS data analysis. In all cases linear dependences were observed, characterized by a slope of about -75 mV dec^{-1}. The parallelism of E vs. log R_F^{-1} dependences once again points out to the surface roughness effect as the main reason for slight differences in apparent HER activity among the Ru/Ti_2AlC electrodes.

3.6. Polarization curves for the HER

Steady-state polarization curves for the HER recorded on the Ru/Ti_2AlC samples in 1.0 mol dm^{-3} H_2SO_4 at 25 °C are shown in Fig. 11a. All samples exhibited very high catalytic activity for the HER, reaching a cathodic current density of -100 mA cm^{-2} in the narrow range of overpotentials between -126 mV (Ru5) and -97 mV (Ru15). The polarization curves for all investigated samples are characterized by a Tafel slope of about -60 mV dec^{-1} at cathodic current densities higher than -10 mA cm^{-2} (see inset) and an exchange current density of 1-2 mA cm^{-2}. Figure 11b shows the polarization curves normalized to the real surface area of Ru by dividing measured current densities by the corresponding r_f value. Expectedly, after r_f correction the Tafel region segments of the curves are lying close to each other, distributed randomly and independently of the number of electrodeposition cycles. Kinetic parameters for the HER determined from the polarization curves for different Ru/Ti_2AlC samples are listed in Table 3.

The Tafel slope is an inherent kinetic property of the electrode material in a given solution, which allows an assessment of the reaction mechanism. In general, the HER on metallic electrodes in acidic solutions proceeds through a combination of three elementary steps. The primary step is always the electrochemical adsorption of H atoms (Volmer step):

$$M + H^+ + e^- \rightarrow M - H_{ads} \quad (3)$$

which is followed by the electrochemical desorption step (Heyrovsky step):

$$M - H_{ads} + H^+ + e^- \rightarrow M + H_2 \quad (4)$$

and/or the chemical desorption step (Tafel step):

$$M - H_{ads} + M - H_{ads} \rightarrow 2M + H_2 \quad (5)$$

Assuming that the reaction follows the Volmer-Heyrovsky pathway and that hydrogen adsorption takes place under Langmuir conditions, theoretically two different slopes could be observed on the Tafel plots depending on the rate-determining step (RDS) and surface coverage by H_{ads}: only one slope of -120 mV dec^{-1} over the entire overpotential range when the Volmer reaction is a RDS, or -40 mV dec^{-1} at lower overpotentials ($\theta_H \rightarrow 0$) and -120 mV dec^{-1} at higher overpotentials ($\theta_H \rightarrow 1$) when the Heyrovsky step is the rate-determining one. Hence, the presence of a Tafel slope of about -60 mV dec^{-1} cannot be explained by a general HER mechanism. It suggests the existence of an additional step in the mechanism, which controls the overall reaction:

$$M + H^+ + e^- \Leftrightarrow M - H^*_{ads} \quad (6)$$

$$M - H^*_{ads} \rightarrow M - H_{ads} \quad (7)$$

$$M - H_{ads} + H^+ + e^- \Leftrightarrow M + H_2 \quad (8)$$

Step (7) represents the surface chemical rearrangements that involve two adsorbed intermediates possessing the same structure, but different energy levels. For low surface coverage by the inactive H^*_{ads} intermediate, the Volmer step is in quasi-equilibrium and potential dependence of θ_H can be expressed by the following equation:

$$\theta_H = \frac{k_1}{k_{-1}} c_{H^+} \exp\left(-\frac{FE}{RT}\right) \quad (9)$$

in which k_1 and k_{-1} are the rate constants of the forward and backward Volmer reaction, respectively, and c the concentration of H^+ ions in the solution. The overall reaction rate is then:

$$j = -2Fk_2\theta_{\mathrm{H}} = -2Fk_2 \frac{k_1}{k_{-1}} c_{\mathrm{H^+}} \exp\left(-\frac{FE}{RT}\right) \quad (10)$$

where k_2 is the rate constant of the rate-controlling surface rearrangement step. For T = 298 K, it yields a Tafel slope $b_c \approx$ -60 mV dec^{-1}.

There are only few papers in literature regarding the kinetics and mechanism of the HER on metallic Ru in acidic solutions, providing somewhat diverse results. Fleischmann and Grenness [49] studied the HER in 1 mol dm^{-3} H_2SO_4 after depositing Ru onto vitreous carbon and reported the values of the Tafel slope that were close to -60 mV dec^{-1}, but increased to -90 mV dec^{-1} for smaller amounts of electrodeposited Ru. They discovered that the HER rate depended upon the size of the Ru electrocatalyst centers and, similarly to our conclusions, suggested the surface diffusion of hydrogen from one type of site to the other as a rate-determining step. Bagotzky et al. [50] obtained a Tafel slope of -70 mV dec^{-1} for the HER on bulk Ru electrodes in 1 mol dm^{-3} H_2SO_4. In contrast to that, Breiter [51] found that b_c had a value of -120 mV dec^{-1} at larger cathodic current densities on Ru foil electrodes in sulfuric acid solutions and proposed the Volmer mechanism for the HER. The studies performed in HCl solutions also showed higher values of Tafel slopes, *e.g.* -120 mV dec^{-1} for bulk Ru [52] or -140 mV dec^{-1} for the Ru nuclei deposited onto Hg [53]. It seems that a mechanism of the HER on metallic Ru electrodes in acidic media strongly depends on a number of factors, including the cathode preparation method, surface pretreatment and selection of an electrolyte.

The Ru/Ti_2AlC electrodes investigated in the present study exhibited superior catalytic activity for the HER in acidic media compared with other Ru-based cathodes in literature [7,9-14]. Most of the cathodes employing RuO_2 as an electrocatalytic material for the HER attained the current density of -100 mA cm^{-2} in the overpotential range from about -200 mV to -250 mV [9-13], approximately 100 mV negative with respect to Ru/Ti_2AlC. The overpotential at -100 mA cm^{-2} measured on highly porous Ni + RuO_2 composite coatings electrodeposited from NH_4Cl nickel baths with suspended RuO_2 particles was -150 mV in 0.5 mol dm^{-3} H_2SO_4 [7].

Cathodes composed of RuO_x nanoparticles deposited on high surface area TiO_2 nanotube arrays showed the HER overpotential of -190 mV in 1 mol dm^{-3} $HClO_4$ [14]. Such an impressive catalytic performance of the Ru/Ti_2AlC electrodes is comparable to that of commercial Pt/C catalysts [54-57].

Among all the Ru/Ti_2AlC electrodes we can mark sample Ru5 as the most promising cathode for the application in industrial conditions. This sample exhibited a slightly lower activity for the HER than Ru15, but at the same time it possessed a compact microstructure, without the presence of cracks or parts of Ru films that peel off from the substrate, which implies its stability during the long term operation. The employment of Ru/Ti_2AlC electrodes obtained at a lower number of Ru electrodeposition cycles is also economically more favorable, because the amount of costly Ru loaded on the Ti_2AlC substrate in the fabrication procedure is reduced to a minimum. In perspective, the electrocatalytic activity of Ru/Ti_2AlC electrodes can be further improved by depositing nanometer-scale thin films of Ru on porous Ti_2AlC substrates of highly developed surface.

4. Conclusions

In this study conductive Ti_2AlC structures were for the first time used as substrate materials in the electrocatalysis of the HER in acidic media. Their excellent stability under anodic polarization in sulfuric acid solutions was attributed to the formation of a thin, passivating oxide layer on the surface. It was shown that electrocatalytic Ru layers can be electrodeposited onto Ti_2AlC substrates by cycling the potential of Ti_2AlC in the solution containing 0.01 mol dm^{-3} $RuCl_3$ and 0.1 mol dm^{-3} H_2SO_4 at a sweep rate of 20 mV s^{-1}. As the number of cycles increased from 5 to 20, the thickness of the Ru coatings increased from 0.42 μm to 2.8 μm, whereas the real surface area of the Ru/Ti_2AlC samples increased four times. The most compact Ru deposit was obtained for 5 electrodeposition cycles, but as the cycling progressed, cracks

started to appear at the coating surface and the Ru films partially peeled off from the Ti_2AlC substrate.

All Ru/Ti_2AlC electrodes exhibited exceptionally high catalytic activity for the HER in 1.0 mol dm^{-3} H_2SO_4 at 25 °C. At a current density of -100 mA cm^{-2} the HER overpotential recorded on Ru/Ti_2AlC samples varied from -97 mV to -126 mV depending on their surface roughness. The Tafel slope of about -60 mV dec^{-1} observed with all samples at large cathodic current densities was explained by a HER mechanism that predicts the surface rearrangement of adsorbed hydrogen intermediates as a RDS.

Acknowledgement

The authors are indebted to the Ministry of Education, Science and Technological Development of the Republic of Serbia for the financial support of this work through the project No. 172054. The support for XPS measurements from Jožef Stefan Institute, Ljubljana, Slovenia, under bilateral collaboration Project No. 451-03-3095/2014-09/26, is gratefully acknowledged. The authors express their gratitude to H. Gao of Department of Materials Science and Engineering, Texas A&M University, USA, for preparation of Ti_2AlC substrates.

References

[1] E. Zoulias, E. Varkaraki, N. Lymberopoulos, C.N. Christodoulou, G.N. Karagioris, A Review of Water Electrolysis, TCJST 4 (2004) 41.

[2] M. Carmo, D.L. Fritz, J. Mergel, D. Stolten, A comprehensive review on PEM water electrolysis, Int. J. Hydrogen Energ. 38 (2013) 4901.

[3] C. Iwakura, M. Tanaka, S. Nakamatsu, H. Inoue, M. Matsuoka, N. Furukawa, Electrochemical properties of $Ni/(Ni + RuO_2)$ active cathodes for hydrogen evolution in chlor-alkali electrolysis, Electrochim. Acta 40 (1995) 977.

[4] N. Spãtaru, J.-G. Le Helloco, R. Durand, A study of RuO_2 as an electrocatalyst for hydrogen evolution in alkaline solution, J. Appl. Electrochem. 26 (1996) 397.

[5] A.C. Tavares, S. Trasatti, Ni + RuO_2 co-deposited electrodes for hydrogen evolution, Electrochim. Acta 45 (2000) 4195.

[6] R.K. Shervedani, S.H. Kazemi, A. Lasia, H.R.Z. Mehrjerdi, Electrocatalytic behavior of thermally deposited RuO_2 into the microporous Raney nickel electrode (Ni-Zn-P-RuO_2) towards the HER, J. New Mat. Electr. Sys. 8 (2005) 213.

[7] L. Vázquez-Gómez, S. Cattarin, P. Guerriero, M. Musiani, Preparation and electrochemical characterization of Ni + RuO_2 composite cathodes of large effective area, Electrochim. Acta 52 (2007) 8055.

[8] U.Č. Lačnjevac, B.M. Jović, V.D. Jović, V.R. Radmilović, N.V. Krstajić, Kinetics of the hydrogen evolution reaction on Ni-(Ebonex-supported Ru) composite coatings in alkaline solution, Int. J. Hydrogen Energ. 38 (2013) 10178.

[9] R. Kötz, S. Stucki, Ruthenium dioxide as a hydrogen-evolving cathode, J. Appl. Electrochem. 17 (1987) 1190.

[10] T.-C. Wen, C.-C. Hu, Hydrogen and Oxygen Evolutions on Ru-lr Binary Oxides, J. Electrochem. Soc. 139 (1992) 2158.

[11] I.M. Kodintsev, S. Trasatti, Electrocatalysis of H_2 Evolution on RuO_2 + IrO_2 Mixed Oxide Electrodes, Electrochim. Acta 39 (1994) 1803.

[12] L. Chen, D. Guay, A. Lasia, Kinetics of the Hydrogen Evolution Reaction on RuO_2 and IrO_2 Oxide Electrodes in H_2SO_4 Solution: An AC Impedance Study, J. Electrochem. Soc. 143 (1996) 3576.

[13] B. Børresen, G. Hagen, R. Tunold, Hydrogen evolution on $Ru_xTi_{1-x}O_2$ in 0.5 M H_2SO_4, Electrochim. Acta 47 (2002) 1819.

[14] U.Č. Lačnjevac, V.V. Radmilović, V.R. Radmilović, N.V. Krstajić, RuO_x nanoparticles deposited on TiO_2 nanotube arrays by ion-exchange method as electrocatalysts for the hydrogen evolution reaction in acid solution, Electrochim. Acta 168 (2015) 178.

[15] M.W. Barsoum, T. El-Raghy, The MAX Phases: Unique New Carbide and Nitride Materials, Am. Scientist 89 (2001) 334.

[16] M. Radovic, M.W. Barsoum, MAX phases: bridging the gap between metals and ceramics, Am. Ceram. Soc. Bull. 92 (2013) 20.

[17] M.W. Barsoum, The $M_{N+1}AX_N$ phases: A new class of solids: Thermodynamically stable nanolaminates, Prog. Solid State Chem. 28 (2000) 201.

[18] M.W. Barsoum, M. Radovic, in: R.W.C.K.H.J. Buschow, M.C. Flemings, E.J. Kramer, S. Mahajan, P. Veyssiere (Eds.), Encyclopedia of Materials: Science and Technology, Elsevier, Amsterdam, 2004.

[19] M.W. Barsoum, T. El-Raghy, Synthesis and Characterization of a Remarkable Ceramic: Ti_3SiC_2, J. Am. Ceram. Soc. 79 (1996) 1953.

[20] D.J. Tallman, B. Anasori, M.W. Barsoum, A critical review of the oxidation of Ti_2AlC, Ti_3AlC_2 and Cr_2AlC in Air, Mater. Res. Lett. 1 (2013) 115.

[21] S. Basu, N. Obando, A. Gowdy, I. Karaman, M. Radovic, Long-Term Oxidation of Ti2AlC in Air and Water Vapor at 1000-1300 °C Temperature Range, J. Electrochem. Soc. 159 (2012) C90.

[22] M.W. Barsoum, M. Radovic, Elastic and mechanical properties of the MAX phases, Ann. Rev. Mater. Res. 41 (2011) 195.

[23] J. Xie, X. Wang, A. Li, F. Li, Y. Zhou, Corrosion behavior of selected $M_{n+1}AX_n$ phases in hot concentrated HCl solution: Effect of A element and MX layer, Corros. Sci. 60 (2012) 129.

[24] D. Li, Y. Liang, X. Liu, Y. Zhou, Corrosion behavior of Ti_3AlC_2 in NaOH and H_2SO_4, J. Eur. Ceram. Soc. 30 (2010) 3227.

[25] M. Naguib, O. Mashtalir, J. Carle, V. Presser, J. Lu, L. Hultman, Y. Gogotsi, M.W. Barsoum, Two-Dimensional Transition Metal Carbides, ACS Nano 6 (2012) 1322.

[26] M. Naguib, M. Kurtoglu, V. Presser, J. Lu, J. Niu, M. Heon, L. Hultman, Y. Gogotsi, M.W. Barsoum, Two-Dimensional Nanocrystals Produced by Exfoliation of Ti_3AlC_2, Adv. Mater. 23 (2011) 4248.

[27] J. Travaglini, M.W. Barsoum, V. Jovic, T. El-Raghy, The corrosion behavior of Ti_3SiC_2 in common acids and dilute NaOH, Corr. Sci. 45 (2003) 1313.

[28] V.D. Jovic, M.W. Barsoum, Corrosion behavior and passive film characteristics formed on Ti, Ti_3SiC_2 and Ti_4AlN_3 in H_2SO_4 and HCl, J. Electrochem. Soc. 151 (2004) B71.

[29] V.D. Jovic, M.W. Barsoum, B.M. Jovic, A. Ganguly, T. El-Raghy, Corrosion Behavior of Ti_3GeC_2 and Ti_2AlN in 1M NaOH, J. Electrochem. Soc. 153 (2006) B238.

[30] V.D. Jovic, B.M. Jovic, S. Gupta, T. El-Raghy, M.W. Barsoum, Corrosion behavior of select MAX phases in NaOH, HCl and H_2SO_4, Corr. Sci. 48 (2006) 4274.

[31] L. Hu, R. Benitez, S. Basu, I. Karaman, M. Radovic, Processing and characterization of porous Ti_2AlC with controlled porosity and pore size, Acta Mat. 60 (2012) 6266.

[32] P. Gudlur, A. Forness, J. Lentz, M. Radovic, A. Muliana, Thermal and mechanical properties of Al/Al_2O_3 composites at elevated temperatures, Mat. Sci. Eng. A 531 (2012) 18.

[33] M.-S. Zheng, S.-G. Sun, In situ FTIR spectroscopic studies of CO adsorption on electrodes with nanometer-scale thin films of ruthenium in sulfuric acid solutions, J. Electroanal. Chem. 500 (2001) 223.

[34] J.F. Moulder, W.F. Stickle, P.E. Sobol, K.D. Bomben, Handbook of X-Ray Photoelectron Spectroscopy, Physical Electronics Inc., Eden Prairie, Minnesota, USA, 1995.

[35] A.L. Antozzi, C. Bargioni, L. Jacopetti, M. Musiani, L. Vazquez-Gomez, EIS study of the service life of activated cathodes for the hydrogen evolution reaction in the chlor–alkali membrane cell process, Electrochim. Acta 53 (2008) 7410.

[36] V.D. Jović, U. Lačnjevac, B.M. Jović, N.V. Krstajić, Service life test of non-noble metal composite cathodes for hydrogen evolution in sodium hydroxide solution, Electrochim. Acta 63 (2012) 124.

[37] B.M. Jović, U.Č. Lačnjevac, N.V. Krstajić, V.D. Jović, Service life test of the NiSn coatings as cathodes for hydrogen evolution in industrial chlor-alkali electrolysis, Int. J. Hydrogen Energ. 39 (2014) 8947.

[38] M. Dahlqvist, B. Allingr, I.A. Abrikosov, J. Rosen, Phase stability of Ti_2AlC upon oxygen incorporation: A first-principles investigation, Phys. Rev. B 81 (2010) 024111-1.

[39] J. Rosen, M. Dahlqvist, S.I. Simak, D.R. McKenzie, M.M. Bilek, Oxygen incorporation in Ti_2AlC: Tuning of anisotropic conductivity, Appl. Phys. Lett. 97 (2010) 073103-1.

[40] T. Liao, J. Wang, M. Li, Y. Zhou, First-principles study of oxygen incorporation and migration mechanisms in Ti_2AlC, J. Mater. Res. 24 (2009) 3190.

[41] P.O.A. Persson, J. Rosen, D.R. McKenzie, M.M. Bilek, Formation of the MAX-phase oxycarbide $Ti_2AlC_{1-x}O_x$ studied via electron energy-loss spectroscopy and first-principles calculations, Phys. Rev. B 80 (2009) 092102-1.

[42] A. Mockute, M. Dahlqvist, L. Hultman, P.O.A. Persson, J. Rosen, Oxygen incorporation in Ti_2AlC thin films studied by electron energy loss spectroscopy and ab initio calculations, J. Mater. Sci. 48 (2013) 3686.

[43] O. Wilhelmsson, J.-P. Palmquist, E. Lewin, J. Emmerlich, P. Eklund, P.O.Å. Persson, H. Högberg, S. Li, R. Ahuja, O. Eriksson, L. Hultman, U. Jansson, Deposition and characterization of ternary thin films within the Ti–Al–C system by DC magnetron sputtering, J. Cryst. Growth 291 (2006) 290.

[44] S. Hadži-Jordanov, H. Angerstein-Kozlowska, M. Vuković, B. E. Conway, Reversibility and Growth Behavior of Surface Oxide Films at Ruthenium Electrodes, J. Electrochem. Soc. 125 (1978) 1471.

[45] R.D. Armstrong, M. Henderson, Impedance plane display of a reaction with an adsorbed intermediate, J. Electroanal. Chem. 39 (1972) 81.

[46] D.A. Harrington, B.E. Conway, AC impedance of faradaic reactions involving electrosorbed intermediates–I. Kinetic theory, Electrochim. Acta 32 (1987) 1703.

[47] G.J. Brug, A.L.G. Van den Eeden, M. Sluyters-Rehbach, J.H. Sluyters, The analysis of electrode impedances complicated by the presence of a constant phase element. J. Electroanal. Chem. 176 (1984) 275.

[48] A. Lasia, A. Rami, Kinetics of hydrogen evolution on nickel electrodes, J. Electroanal. Chem. 294 (1990) 123.

[49] M. Fleischmann, M. Grenness, Electrocrystallization of Ruthenium and Electrocatalysis of Hydrogen Evolution, J. Chem. Soc., Faraday Trans. 1 68 (1972) 2305.

[50] V.S. Bagotzky, A.M. Skundin, E.K. Tuseeva, Adsorption of hydrogen and oxygen and oxidation of methanol on ruthenium electrodes, Electrochim, Acta 21 (1976) 29.

[51] M.W. Breiter, Hydrogen evolution and dissolution on smooth ruthenium in sulfuric acid solution, J. Electroanal. Chem. 178 (1984) 53.

[52] A.T. Kuhn, P.M. Wright, The cathodic evolution of hydrogen on ruthenium and osmium electrodes, J. Electroanal. Chem. 27 (1970) 319.

[53] R.D. Giles, J.A. Harrison, H.R. Thirsk, Catalytic hydrogen evolution on ruthenium and platinum nuclei, J. Electroanal. Chem. 20 (1969) 47.

[54] W.-F. Chen, K. Sasaki, C. Ma, A.I. Frenkel, N. Marinkovic, J.T. Muckerman, Y. Zhu, R.R. Adzic, Hydrogen-Evolution Catalysts Based on Non-Noble Metal Nickel–Molybdenum Nitride Nanosheets, Angew. Chem. Int. Ed. 51 (2012) 6131.

[55] X. Chen, D. Wang, Z. Wang, P. Zhou, Z. Wu, F. Jiang, Molybdenum phosphide: a new highly efficient catalyst for the electrochemical hydrogen evolution reaction, Chem. Commun. 50 (2014) 11683.

[56] L. Lang, Y. Shi, J. Wang, F.-B. Wang, X.-H. Xia, Hollow Core−Shell Structured Ni−Sn@C Nanoparticles: A Novel Electrocatalyst for the Hydrogen Evolution Reaction, ACS Appl. Mater. Interfaces 7 (2015) 9098.

[57] L. Ma, L.R.L. Ting, V. Molinari, C. Giordano, B.S. Yeo, Efficient hydrogen evolution reaction catalyzed by molybdenum carbide and molybdenum nitride nanocatalysts synthesized via the urea glass route, J. Mater. Chem. A 3 (2015) 8361.

Figure captions:

Fig. 1. Polarization curve recorded on Ti_2AlC in 1.0 mol dm^{-3} H_2SO_4 at 25 °C by sweeping the potential from -1.0 V to 2.0 V at a rate of 1 mV s^{-1}.

Fig. 2. XPS depth profiles of concentration of different elements (marked in the figure) obtained for the surface of: (a) as-prepared Ti_2AlC and (b) Ti_2AlC subjected to the potential of 2.0 V in 1.0 mol dm^{-3} H_2SO_4 for 1 h.

Fig. 3. XPS spectra of: (a) C 1s, (b) Ti 2p and (c) Al 2p obtained from the surface of non-treated and anodically treated (oxidized) Ti_2AlC samples.

Fig. 4. CVs of Ru electrodeposition onto Ti_2AlC substrates recorded in the potential range from -0.5 V to 0.4 V at a sweep rate of 20 mV s^{-1} during the preparation of samples: (a) Ru5 and (b) Ru20 (cycle numbers are marked in the figure). Solution: 0.01 mol dm^{-3} $RuCl_3$ + 0.1 mol dm^{-3} H_2SO_4. Inset: enhancement of voltammetric responses at potentials positive than -0.25 V during the repetitive cycles of Ru deposition.

Fig. 5. Morphology of different Ru/Ti_2AlC samples: Ru5 – (a) and (b); Ru10 – (c) and (d); Ru15 – (e) and (f); Ru20 – (g) and (h).

Fig. 6. AFM analysis of Ru coating thickness. Sample Ru5: (a) surface plot, (b) and (c) section analysis (25 μm x 25 μm x 3.5 μm); sample Ru20: (e) surface plot, (f) and (g) section analysis (35 μm x 35 μm x 4 μm).

Fig. 7. CVs recorded on different Ru/Ti_2AlC samples in 1.0 mol dm^{-3} H_2SO_4 at 25 °C by applying a sweep rate of 20 mV s^{-1} in the potential range from -0.25 V to 0.4 V corresponding to reversible Ru oxide formation at the surface: (a) measured CVs; (b) CVs after correction for the surface roughness factor (r_f). The total number of electrodeposition cycles for each sample is marked in the figure.

Fig. 8. Nyquist plots recorded at the potentials of: (a) -0.28 V and (b) -0.34 V for all Ru/Ti_2AlC samples (marked in the figure), and (c) Nyquist plots recorded on sample Ru15 at five different potentials (marked in the figure).

Fig. 9. Equivalent circuits applied for fitting the impedance spectra for the HER recorded at (a) less negative and (b) more negative potentials.

Fig. 10. Potential dependences of: (a) the double layer capacitance, C_{dl}, and (b) the total faradaic resistance to the HER, R_F, obtained from the EIS analysis for different Ru/Ti_2AlC samples (marked in the figure).

Fig. 11. (a) Polarization curves for the HER recorded on different Ru/Ti_2AlC samples (marked in the figure) in 1.0 mol dm^{-3} H_2SO_4 at 25 °C. Inset: linear fits of the polarization curves in the range of current densities higher than -10 mA cm^{-2} (Tafel slopes). (b) The same polarization curves corrected for the roughness factor r_f.

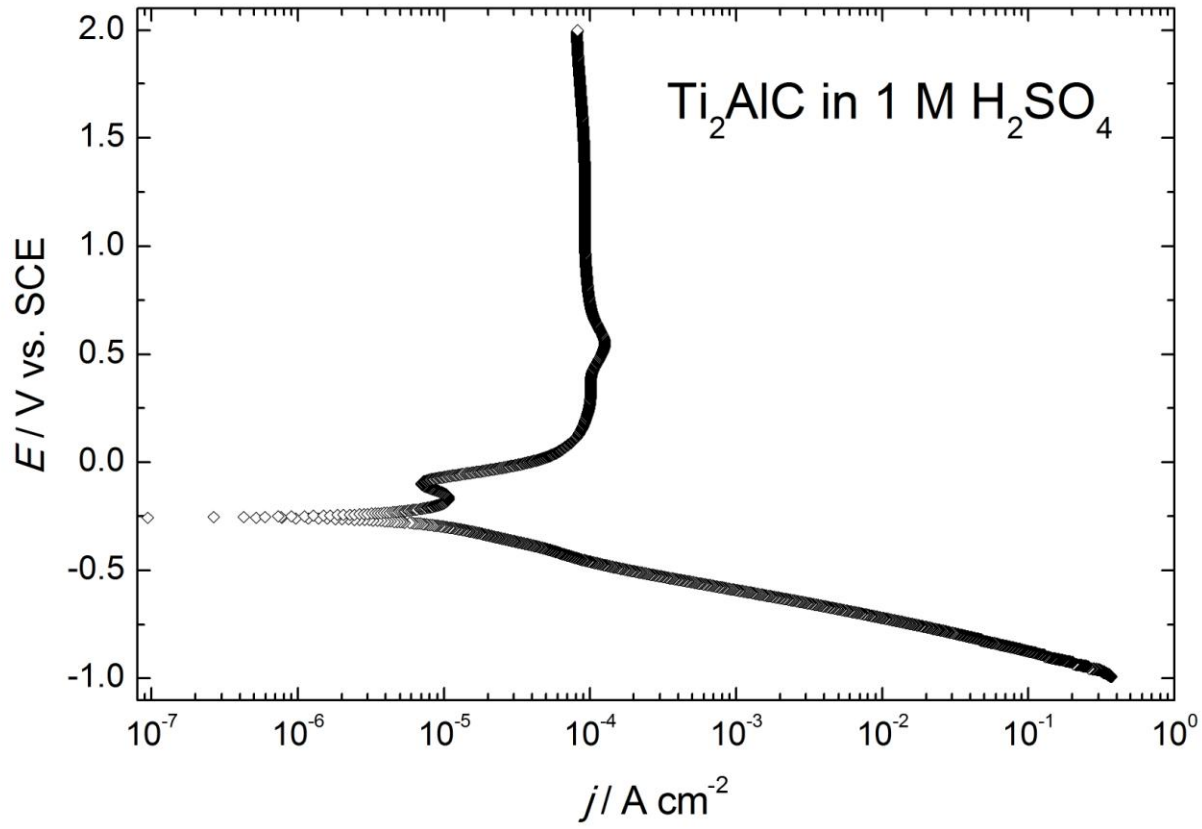

Fig. 1

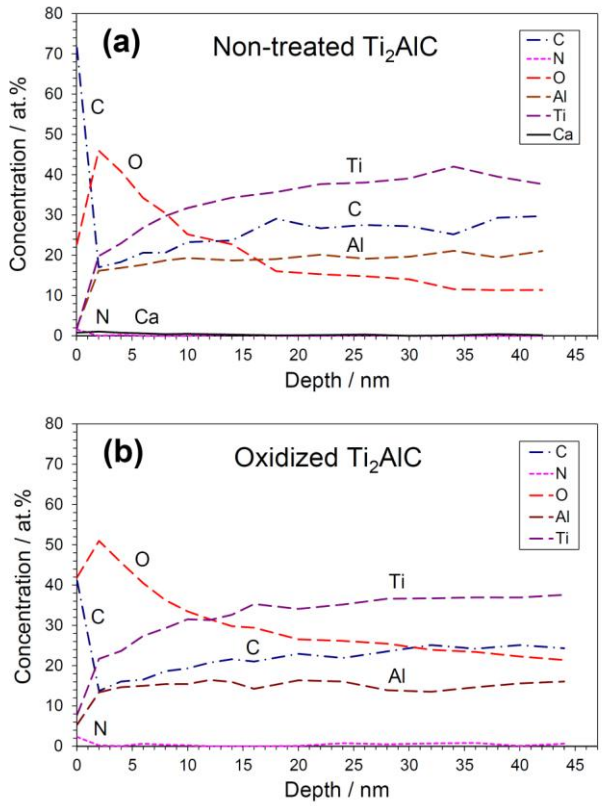

Fig. 2

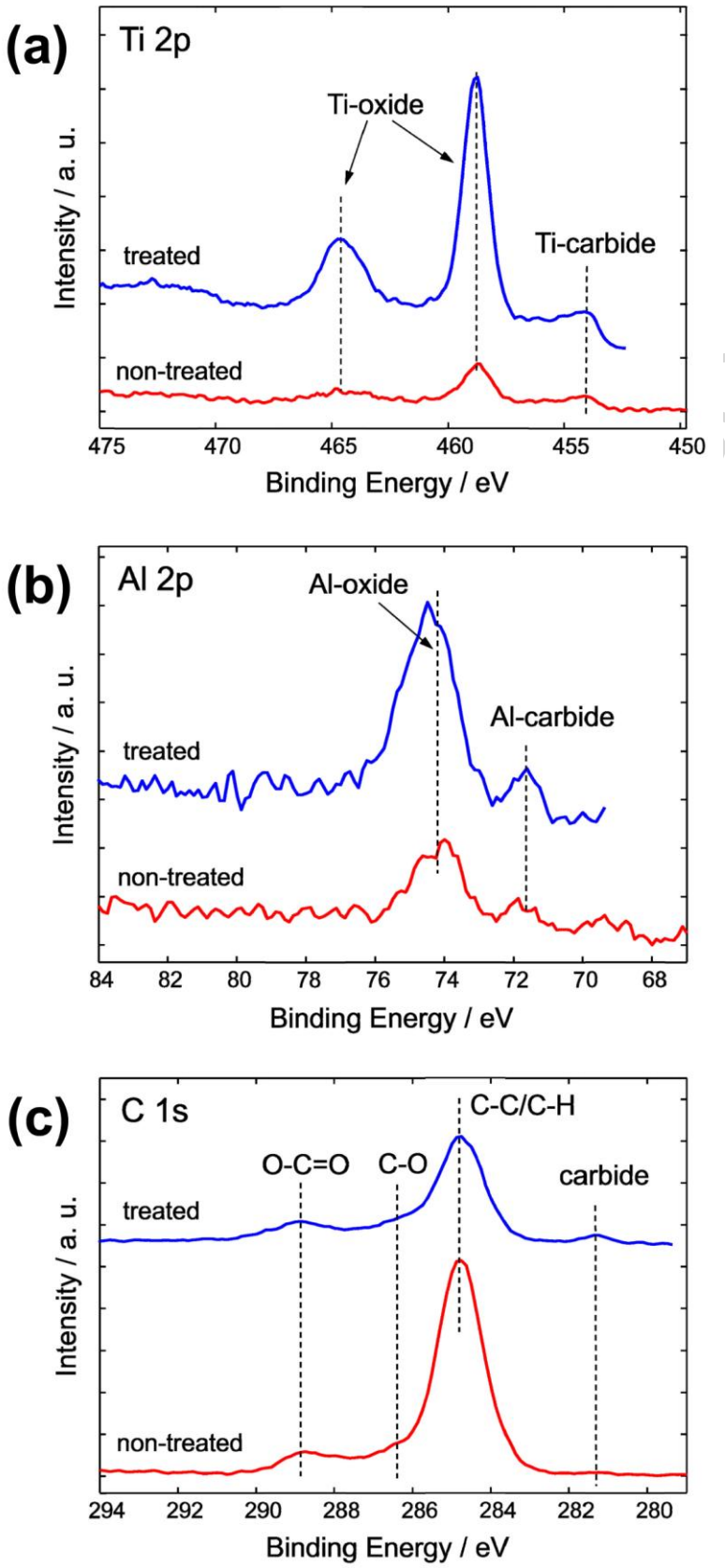

Fig. 3

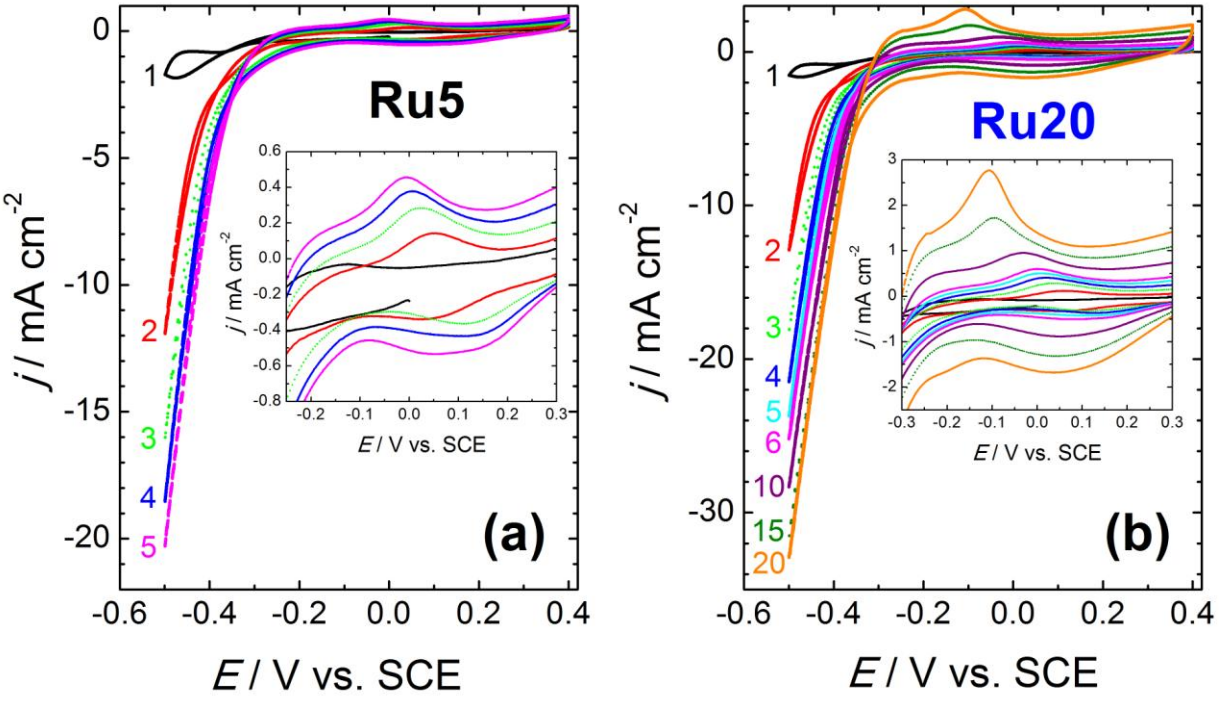

Fig. 4

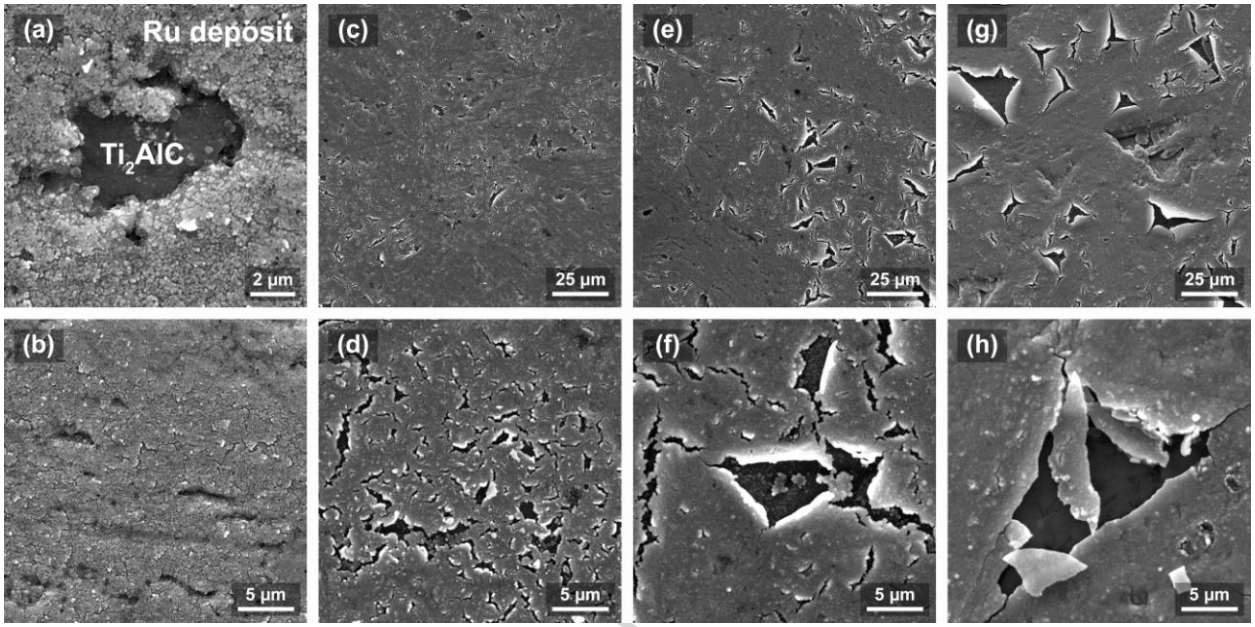

Fig. 5

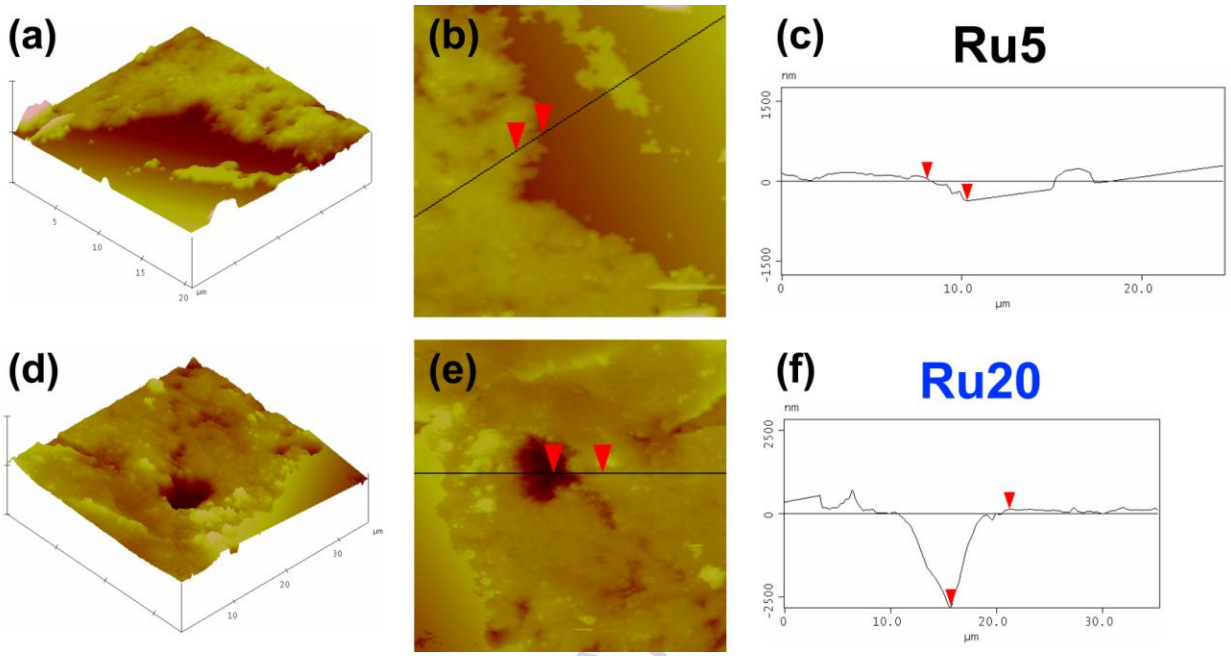

Fig. 6

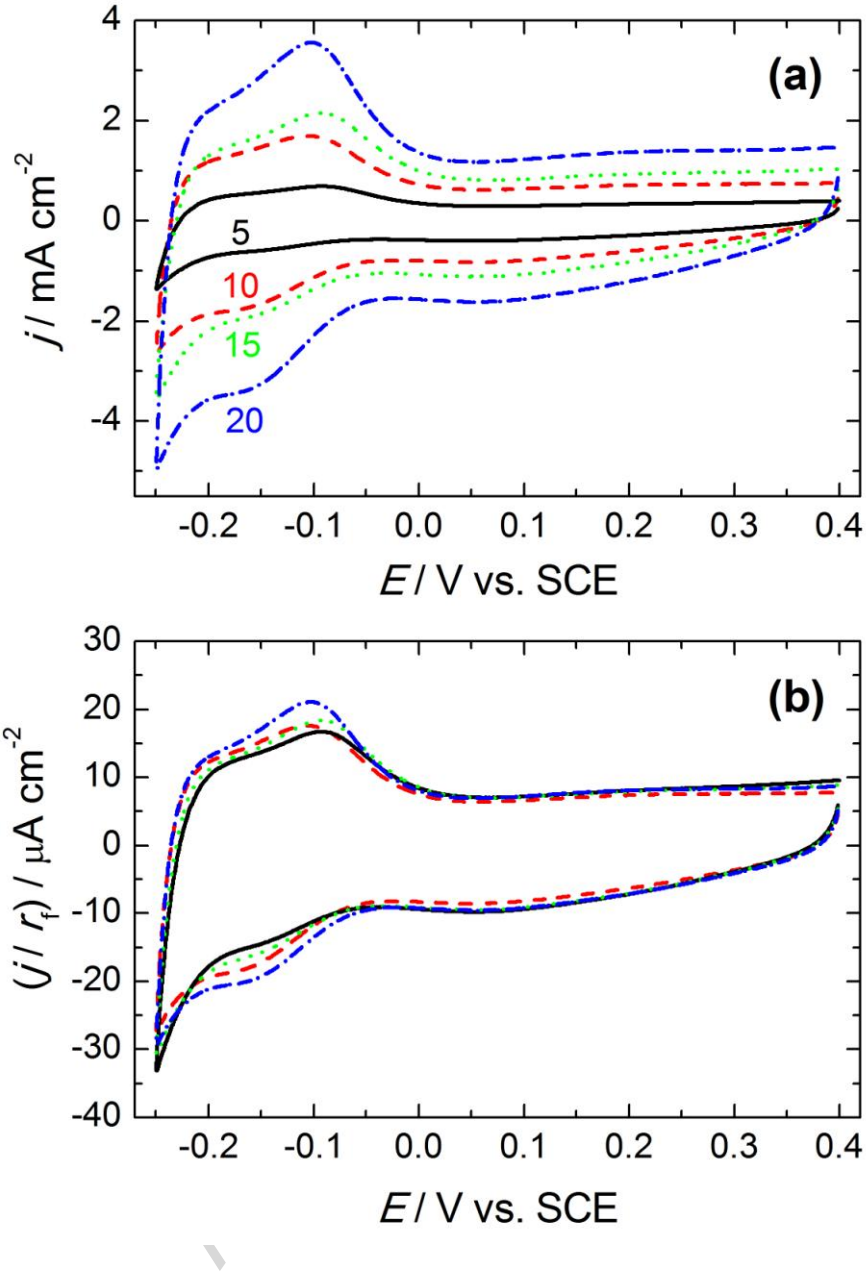

Fig. 7

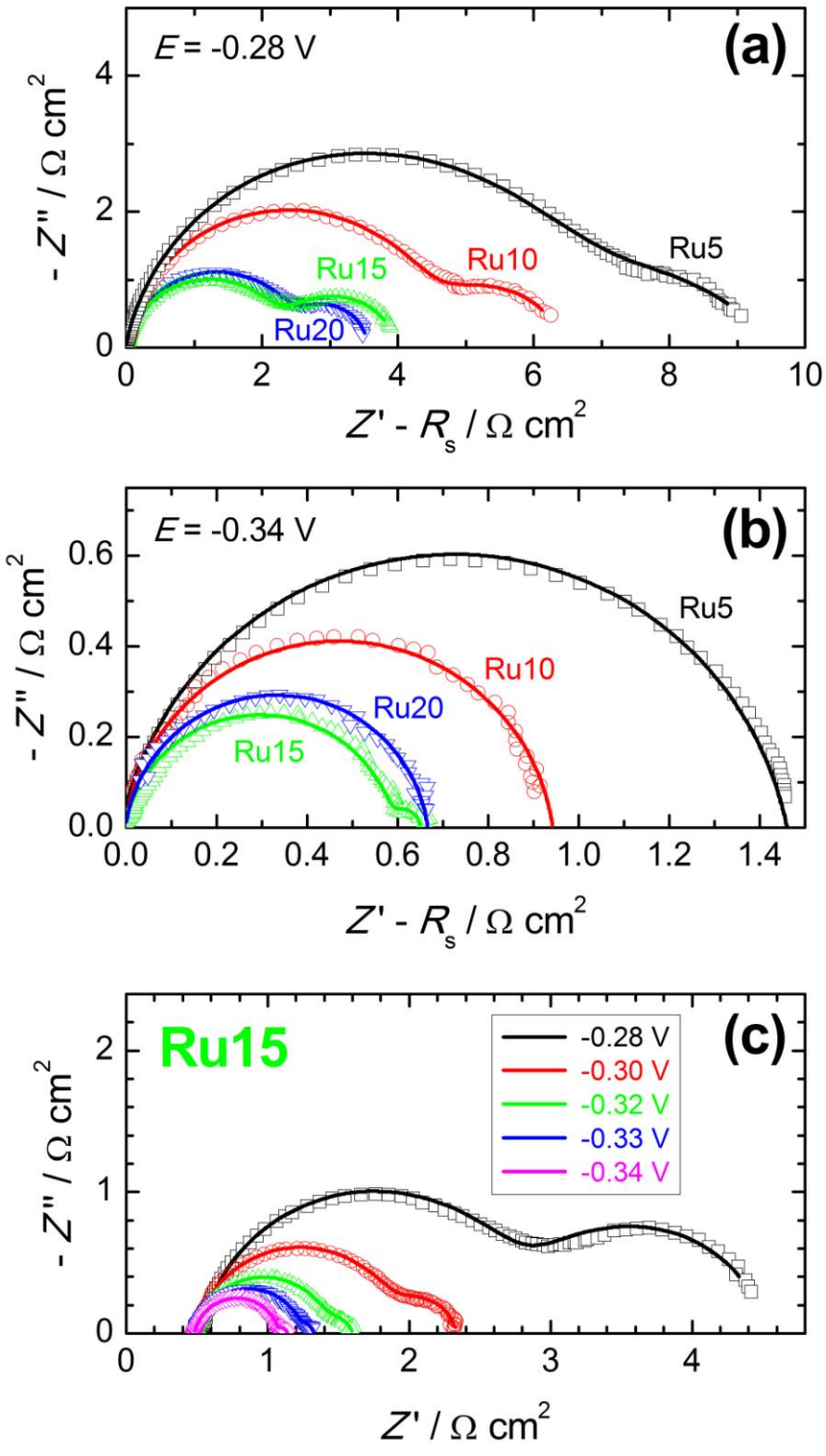

Fig. 8

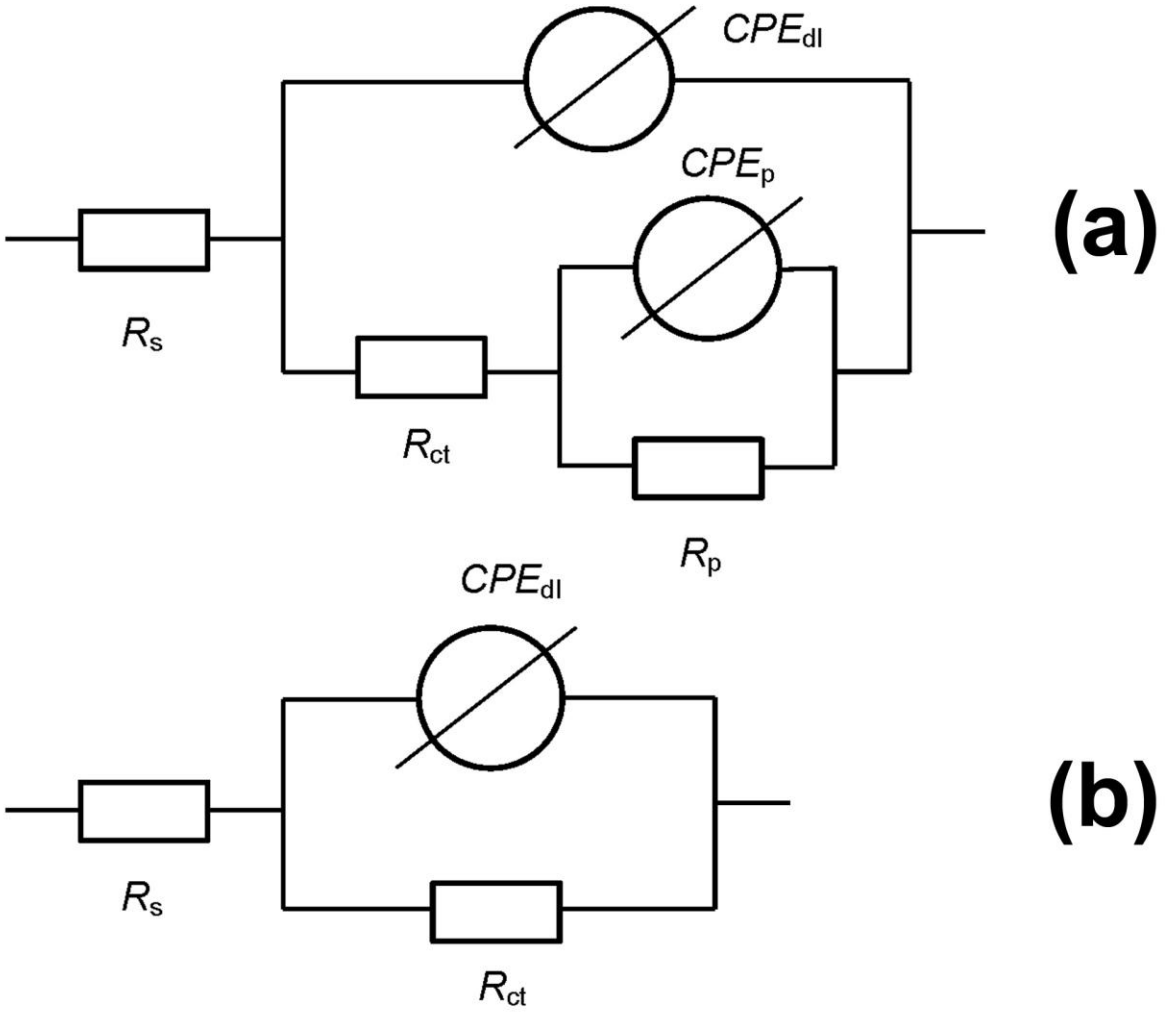

Fig. 9

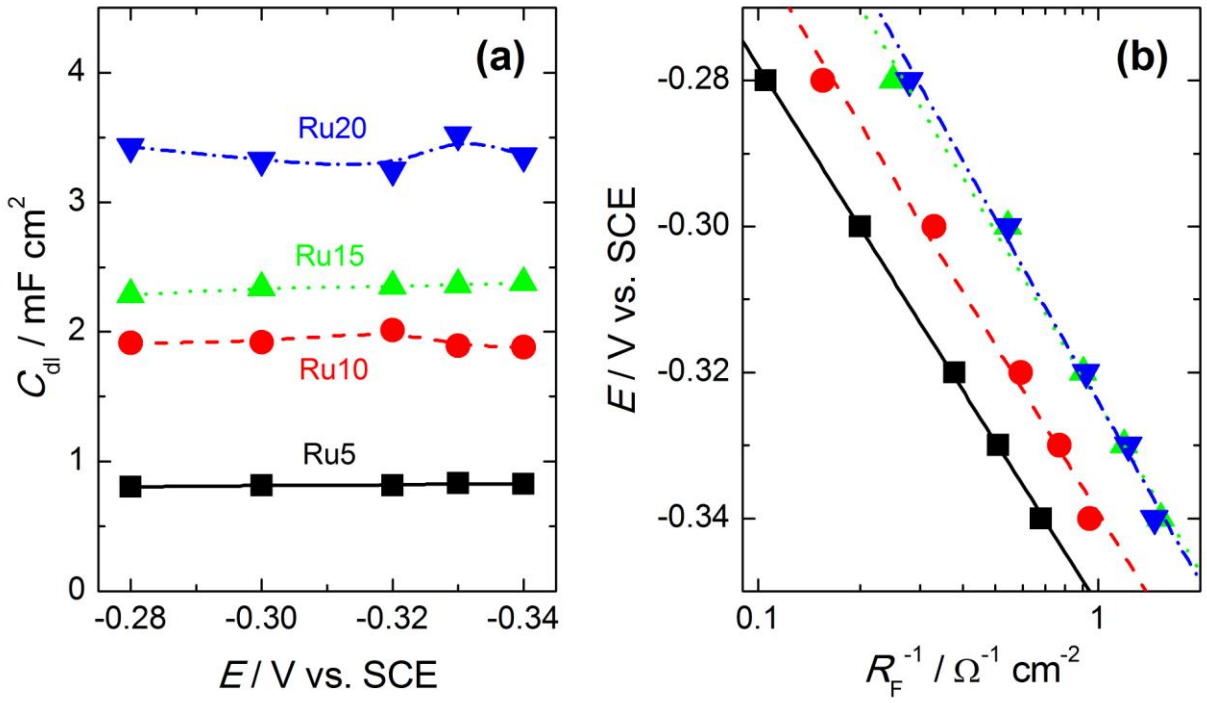

Fig. 10

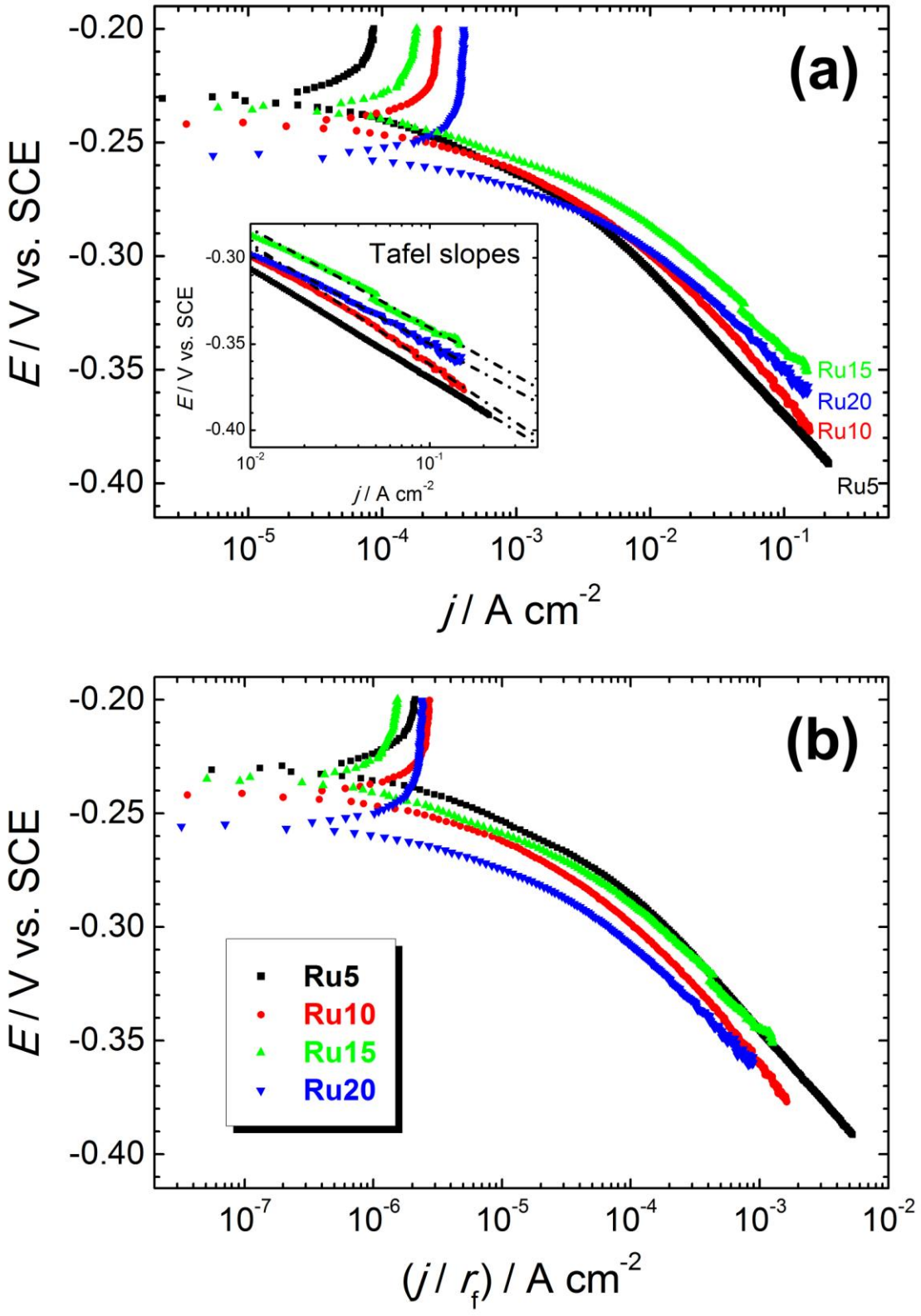

Fig. 11

Table 1: The average thickness of Ru films on Ti_2AlC determined from AFM analysis (d_{av}) and the roughness factor of Ru/Ti_2AlC samples obtained from EIS analysis (r_f).

Sample	d_{av} / μm	r_f
Ru5	0.42	41
Ru10	1.85	96
Ru15	2.45	117
Ru20	2.82	169

Table 2: Parameters obtained from modeling the EIS spectra of various Ru/Ti_2AlC samples using the equivalent circuits presented in Fig. 9.

Sample	E / V	R_s / Ω cm^2	R_p / Ω cm^2	Y_p / mS cm^{-2} s^{α}	α_p	R_{ct} / Ω cm^2	Y_{dl} / mS cm^{-2} s^{α}	α_{dl}
Ru5	-0.28	0.52	2.84	1.6	0.621	6.66	2.0	0.883
	-0.30	0.52	1.14	1.9	0.520	3.87	1.9	0.893
	-0.32	0.50	-	-	-	2.64	2.4	0.866
	-0.33	0.50	-	-	-	1.97	2.3	0.873
	-0.34	0.50	-	-	-	1.47	2.3	0.875
Ru10	-0.28	0.76	1.76	3.0	0.835	4.70	3.7	0.902
	-0.30	0.78	0.35	9.9	0.800	2.68	3.9	0.897
	-0.32	0.82	0.12	7.4	0.860	1.58	3.5	0.917
	-0.33	0.80	-	-	-	1.26	3.7	0.904
	-0.34	0.80	-	-	-	1.17	2.3	0.875
Ru15	-0.28	0.53	1.61	2.5	0.859	2.40	5.2	0.881
	-0.30	0.49	0.38	3.9	0.927	1.47	5.5	0.880
	-0.32	0.49	0.17	7.0	0.825	0.94	5.1	0.892
	-0.33	0.49	0.08	1150	0.889	0.75	5.4	0.886
	-0.34	0.48	0.06	2600	0.999	0.60	5.6	0.884
Ru20	-0.28	0.70	0.95	3.2	0.960	2.63	6.9	0.890
	-0.30	0.65	-	-	-	1.60	7.4	0.877
	-0.32	0.67	-	-	-	1.01	7.9	0.867
	-0.33	0.67	-	-	-	0.76	5.4	0.936
	-0.34	0.65	-	-	-	0.68	7.0	0.892

Table 3: Kinetic parameters for the HER on different Ru/Ti_2AlC samples obtained from the polarization curves presented in Fig. 11: the Tafel slope, b_c, exchange current density, j_0, overpotential corresponding to the current density of –100 mA cm^{-2}, η_{100}, and the area-specific activity at the overpotential of –100 mV, $(j / r_f)_{100}$.

Sample	b_c / mV dec^{-1}	j_0 / mA cm^{-2}	η_{100} / mV	$(j / r_f)_{100}$ / mA cm^{-2}
Ru5	–64	1.1	–126	–0.96
Ru10	–70	2.1	–117	–0.59
Ru15	–58	2.1	–97	–0.96
Ru20	–56	1.3	–106	–0.46

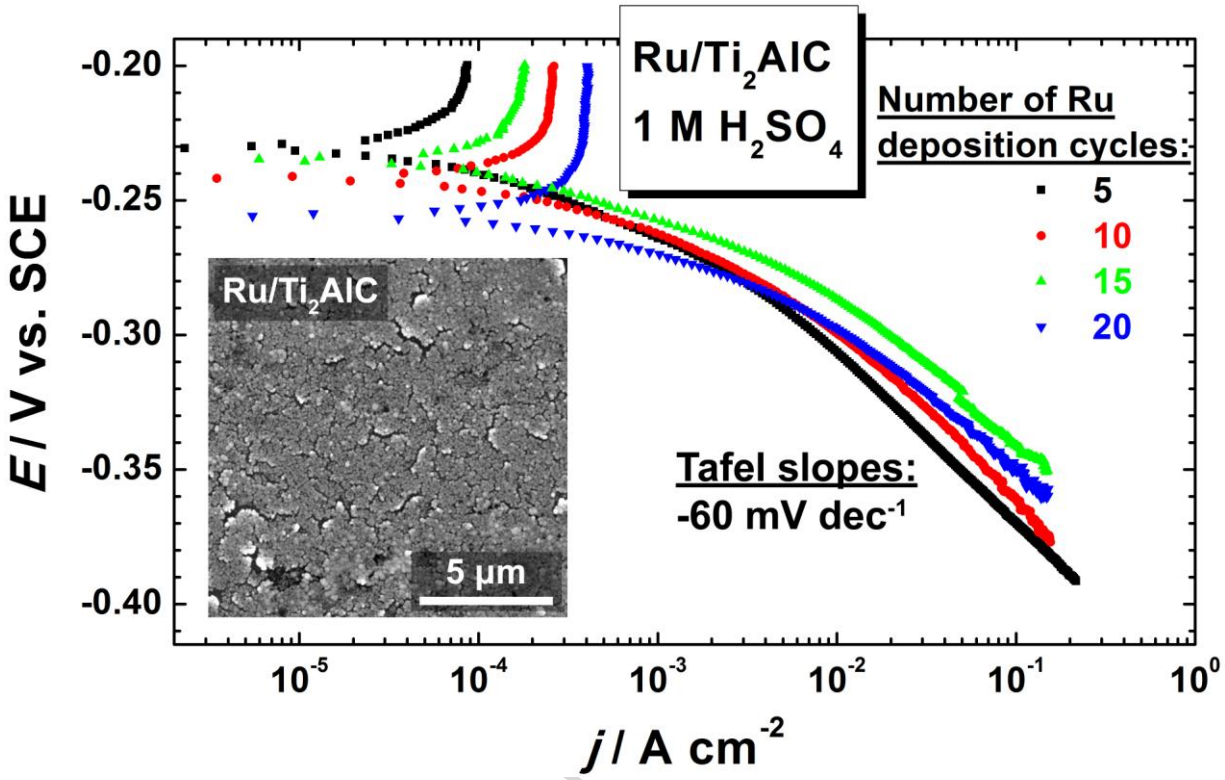

Graphical abstract

Research Highlights

► Ti_2AlC was examined as a substrate material for HER electrocatalysts in acid media.

► It showed excellent stability at high anodic potentials in H_2SO_4 solutions.

► Ru films were deposited by cycling the potential of Ti_2AlC in $RuCl_3$ + H_2SO_4 solution.

► Thickness of Ru films varied from 0.42 to 2.8 μm depending on the number of cycles.

► All Ru/Ti_2AlC electrodes were exceptionally active for HER in 1 M H_2SO_4 at 25°C.